Aircraft Engineering and Aerospace Technology

Simulation of dynamic stall using direct-forcing immersed boundary method at low Reynolds number

Nima Vaziri, Ming-Jyh Chern, Tzyy-Leng Horng,

Simulation of dynamic stall using direct-forcing immersed boundary method at low Reynolds number

Nima Vaziri
Department of Physics, Karaj Branch, Islamic Azad University, Karaj, Iran
Ming-Jyh Chern
Department of Mechanical Engineering, National Taiwan University of Science and Technology, Taipei, Taiwan, and
Tzyy-Leng Horng
Department of Applied Mathematics, Feng Chia University, Taichung, Taiwan

Abstract

Purpose – The purpose of this study is simulation of dynamic stall behavior around the Eppler 387 airfoil in the low Reynolds number flow with a direct-forcing immersed boundary (DFIB) numerical model.

Design/methodology/approach – A ray-casting method is used to define the airfoil geometry. The governing continuity and Navier–Stokes momentum equations and boundary conditions are solved using the DFIB method.

Findings – The purposed method is validated against numerical results from alternative schemes and experimental data on static and oscillating airfoil. A base flow regime and different vortices patterns are observed, in accordance with other previously published investigations. Also, the effects of the reduced frequency, the pitch oscillation amplitude and the Reynolds number are studied. The results show that the reduced frequency has a major effect on the flow field and the force coefficients of the airfoil. On the other hand, the Reynolds number of the flow has a little effect on the dynamic stall characteristics of the airfoil at least in the laminar range.

Practical implications – It is demonstrated that the DFIB model provides an accurate representation of dynamic stall phenomenon.

Originality/value – The results show that the dynamic stall behavior around the Eppler 387 is different than the general dynamic stall behavior understanding in the shedding phase.

Keywords Direct-forcing immersed boundary method

Paper type Research paper

Introduction

Dynamic retreating blade stall problem is one of the well-known limiting factors of high-speed characteristics of a rotary wing aircraft. When an airfoil is pitching up, the flow separation and separation-vortex shedding is delayed, resulting in a higher maximum lift coefficient. When the airfoil reaches the end of its angle and starts to pitch down, the separation-vortex is generally rapidly shed from the airfoil, causing enormous drop in lift. The critical angle of attack for the stall is about 15°, but it may vary significantly depending on the airfoil and the Reynolds number. McCroskey and his colleagues investigated the details of the dynamic stall phenomenon (Ko and McCroskey, 1997; McCroskey, 1981, 1982) for more than two decades. Also, many experimental (Ohmi *et al.*, 1991; Lee and Gerontakos, 2004; Gardner *et al.*, 2016) and numerical (Akbari and Price, 2003; Wang *et al.*, 2010; Mohan *et al.*, 2016) studies have been reported in this area.

The most common method to simulate the flow with a complicated solid boundary is to use a body-fitted technique with grids fitting and clustering along the complex boundary. Most of time, the solid object may not be at rest, and it requires further technique to deal with a moving object. The mesh updating or re-meshing is usually computationally expensive. The immersed boundary (IB) method (Peskin, 1972) is a numerical method for the simulation of fluid–structure interaction problems. The main capability of IB is to handle simulations of a moving boundary with less computational cost and memory requirements than the conventional body-fitted method, especially in low Reynolds number problems. In this method, a fixed Cartesian grid is used for fluids, and a Lagrangian grid is applied for the immersed solid object. Instead of using a delta function, Mohd-Yusof (1996) introduced the direct-forcing immersed boundary (DFIB) method. In this method, a virtual forcing term is determined by the difference between the interpolated velocities at the boundary points and the desired boundary velocities. The idea of DFIB has been used and developed successfully in many

The current issue and full text archive of this journal is available on Emerald Insight at: **www.emeraldinsight.com/1748-8842.htm**

Aircraft Engineering and Aerospace Technology
© Emerald Publishing Limited [ISSN 1748-8842]
[DOI 10.1108/AEAT-05-2017-0128]

Received 18 May 2017
Revised 15 December 2017
22 December 2017
Accepted 23 December 2017

studies (Noor *et al.*, 2009; Chern *et al.*, 2014; Belliard *et al.*, 2016; Eshghinejadfard *et al.*, 2016; Delouei *et al.*, 2016).

The present study describes a DFIB model (following Chern *et al.*, 2015) of the dynamic stall behavior for the Eppler 387 (E387) airfoil. Low-Reynolds-number aerodynamics and airfoils (like the E387) are important in applications such as small airplanes, sailplanes, wind turbines and propellers. There are plenty of studies about the static stall behavior of the E387 airfoil (McGhee *et al.*, 1988; Shahin *et al.*, 2008); but based on the authors' knowledge, there is no investigation about the dynamic stall phenomenon of this airfoil. Also, The NACA 0012 airfoil is used for some validation cases. The solid object immersed within a flow field is denoted by the volume of solid function η. A cell occupied by solids will be denoted as $\eta = 1$, while the one fully occupied by fluids will be $\eta = 0$. A ray-casting algorithm (Sutherland *et al.*, 1974) is used to define the airfoil geometry and find the value of η. The aim of the present work is the study of the capability of the DFIB method as a distinguished numerical method on a complex geometry in handling fluid–solid interactions. Also, the effects of the main parameters on the dynamic stall of the E387 airfoil are studied. It should be noted that the present study is in two-dimensional domain and also just valid for low-Reynolds-number cases.

Mathematical formulae and numerical methods

The governing equations for an incompressible Newtonian fluid are represented in the following non-dimensional forms as:

$$\nabla \cdot \mathbf{u} = 0, \tag{1}$$

$$\frac{\partial \mathbf{u}}{\partial t} + \nabla \cdot (\mathbf{uu}) = -\nabla p + \frac{1}{Re}\nabla^2 \mathbf{u} + \eta \mathbf{f}, \tag{2}$$

where $\mathbf{u}$ and p are non-dimensional velocity and pressure, respectively; $\mathbf{u}$ is nondimensionalized by the inlet free stream velocity ($\mathbf{u}_\infty$). Also, $\eta\mathbf{f}$ shows the virtual force only applied to solids. The forcing term $\mathbf{f}$ is determined by the difference between the interpolated velocity on the boundary point and the desired boundary velocity. It is defined by:

$$\mathbf{f} = \frac{\mathbf{u}* - \mathbf{u}**}{\Delta t}, \tag{3}$$

where $\mathbf{u}^\star$ and $\mathbf{u}^{\star\star}$ are denoted as the velocity at the center of the solid geometry and the second intermediate velocity, respectively.

Numerical method

A staggered grid arrangement is used in this study. The second-order central difference scheme and the third-order quadratic upstream interpolation for convective kinetics scheme (Leonard, 1979) are used to discretize the diffusive and the convective terms of equation (2), respectively. Also, the Adam–Bashforth scheme is used for temporal terms.

The integration of virtual force is used to calculate the resultant force exerted on the solid object by fluid:

$$\mathbf{F} = -\iiint_{cv} \eta \mathbf{f} dV, \tag{4}$$

where the control volume is around the solid geometry. The dimensionless drag and lift force coefficients, C_D and C_L, can be denoted as:

$$C_D = 2\mathbf{F_x}, \tag{5}$$

and:

$$C_L = 2\mathbf{F_y}, \tag{6}$$

respectively. Full details of the discretized equations are given by Chern *et al.* (2014, 2015).

Ray-casting algorithm

The ray-casting method is used to define a solid part of the computational domain in the present study. In this algorithm, first the geometry of the solid should be defined by connection of the points that create it. Next, the separation of the solid and the fluid sections is accomplished by the ray-casting algorithm, which is one of the point-in-polygon methods. The ray-casting algorithm tests how many times a ray, starting from the point and moving in any fixed direction, intersects the edges of the solid geometry. The ray intersects the edge an odd number of times if the point is on the inside of the solid section. Also, for the outside points, the ray intersects its edge even (or zero) number of times. A pseudocode can be written as:

```
count ← 0
foreach side in polygon:
  if ray_int._seg.(P, side) then
   count ← count + 1
if is_odd (count) then
  return inside
else
  return outside
```

The function "ray_int._seg." is true if the horizontal ray starting from the point P intersects the side (segment), false otherwise. In the present study, the airfoil is defined with X-Y coordinates in a geometry data file. The solid part is specified with the ray-casting algorithm. Figure 1 shows an example of the method. After defining the airfoil, all points of the domain are checked by the ray-casting algorithm. More details can be found in a study published by Sutherland *et al.* (1974).

Pitching airfoil

In the dynamic stall cases, a pitching airfoil is considered. The instantaneous angle of attack (AOA) is given by:

$$\alpha = \alpha_{\text{mean}} + \alpha_{\text{amp}} \sin(2\pi f t), \tag{7}$$

Figure 1 Example of the ray-casting algorithm to separate the solid and fluid parts

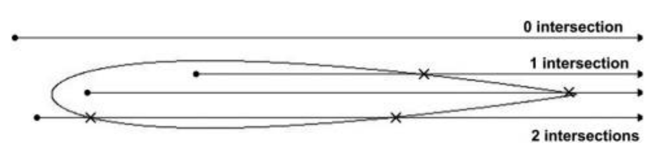

where α_{mean}, α_{amp} and f represent the mean angle of attack, the pitch oscillation amplitude and the oscillation frequency, respectively. Also, the reduced frequency is defined as:

$$k = \frac{\pi f c}{U_\infty}, \tag{8}$$

Results and discussion

The simulation results and the parameter studies of the dynamic stall flow are presented in this section. A full description is given by Chern *et al.* (2015) of the basic computational model (without the ray-casting section) validation for a heated circular cylinder placed in an unbounded uniform flow investigated by many researchers.

The first two cases of this section are validations of the present model in the static stall mode of the NACA 0012 and the Eppler 387 airfoils. Next, the dynamic stall flow of the NACA 0012 airfoil studied and the flow field is compared with former results. Then, the E387 airfoil is considered. The dynamic stall behavior and the effect of three main parameters of that are investigated and discussed.

Case 1: static airfoil – NACA 0012

The typical geometric set up in the computational domain is shown in Figure 2. The Dirichlet boundary condition is applied at the inlet boundary, and Neumann boundary conditions are applied at lateral and outlet sides. In this case, the drag and lift coefficients are predicted at $\alpha = 8°$ for Reynolds number Re = 50,000 for a NACA 0012 airfoil. Table I lists the parameters used to test for mesh and size convergence test. It may be observed from Table I that the predicted drag and lift coefficients are almost insensitive to the number of grid points, except for the two cases. The minimum size of the domain with reasonable results is $8c$ X $4c$. Also, for all next cases, the grids number 1000X1000 are chosen. It should be noted that all the present study cases are simulated in low Reynolds number flow. Based on the previous studies and general understanding in this area, larger computational domains are needed for high Reynolds number flow simulation. The non-dimensional time step for all cases is 10^{-4} and the CFL number is 0.0125 for the selected domain and grid size. The simulation is performed on a workstation with two 3.40 GHz CPU and 3 GB RAM and required less than 10 h CPU time to compute results up to a non-dimensional time ($t^* = t\,\mathbf{u}_\infty/c$) of 2. Figure 3 shows the non-dimensional pressure contours around the airfoil, which is in agreement with general understanding in this area.

Figure 2 Typical computational domain

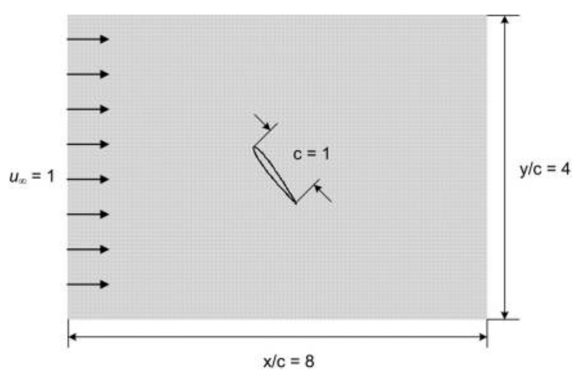

Case 2: static airfoil – Eppler 387

In the second static condition case, the E387 airfoil with Re = 60,000 is considered. Drag and lift coefficients are computed in different angles of attacks from −2° to 12°. Figures 4 and 5 show the comparisons of the present study with the

Figure 3 Non-dimensional pressure contours around the NACA 0012 airfoil

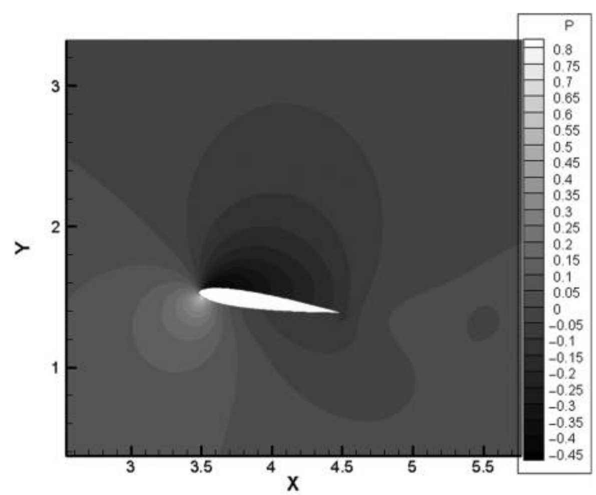

Notes: $\alpha = 8°$; Re = 10,000

Table I Mesh convergence test results

Domain size	Grid resolution	C_L	C_D	Abs. error of C_L (%)	Abs. error of C_D (%)
16c × 16c	2,000 × 2,000	0.835	0.0421	0.238	0.237
16c × 8c	2,000 × 1,000	0.835	0.0420	0.238	0.473
4c × 4c	500 × 500	0.707	0.0322	18.387	31.055
8c × 4c	500 × 500	0.780	0.0381	6.810	9.716
8c × 4c	1,000 × 500	0.803	0.0408	4.062	3.317
8c × 4c	1,000 × 1,000	0.830	0.0418	0.836	0.948
8c × 4c	1,500 × 750	0.829	0.0419	0.955	0.711
8c × 4c	2,000 × 2,000	0.835	0.0420	0.238	0.473
–	Xfoil code	0.837	0.0422	–	–

Figure 4 Drag coefficient at steady angles of attack for Re = 60,000

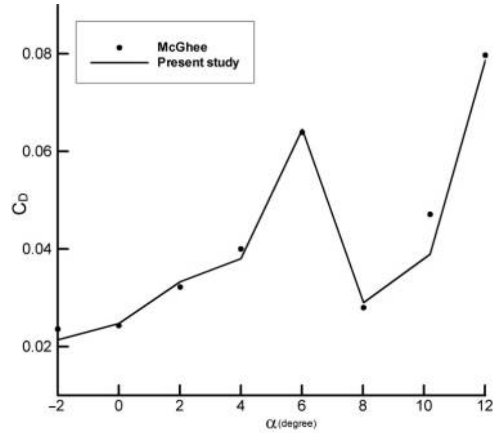

Notes: –: present study; ●: experimental results due to McGhee *et al.* (1988)

Figure 5 Lift coefficient at steady angles of attack for Re = 60,000

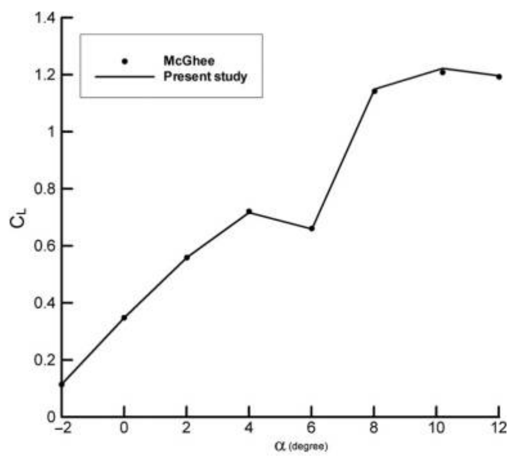

Notes: –: present study; ●: experimental results due to McGhee *et al.* (1988)

experimental results of McGhee *et al.* (1988). It can be seen that both of them are close to the experimental results.

Case 3: dynamic stall – NACA 0012

In the first dynamic stall cases, the oscillations of NACA 0012 airfoil with k = 0.25, Re = 10,000, α_{mean} = 5° and α_{amp} = 20° are considered. The pitching oscillation of the airfoil starts from the minimum value and the oscillation cycle is completed during the simulation based on the equation (7). Dynamic lift and drag loops are depicted in Figures 6 and 7. The results are compared with outcomes of Tuncer *et al.* (1990) and the simulation results of Akbari and Price (2003). It can be seen that an almost good similarity is observed between the present study and the former results. The maximum lift and drag coefficients of the present simulation are higher than those reported by Akbari and Price (2003). Also, the lift coefficient is decreased dramatically after the maximum angle of attack.

Figure 6 Lift coefficients versus angle of attack for the NACA 0012 airfoil

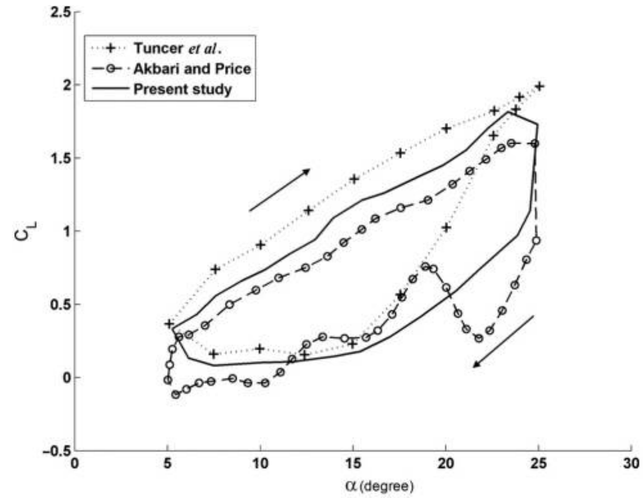

Notes: k = 0.25, Re = 10,000, α_{mean} = 5° and α_{amp} = 20°; –: present study; ..+..: Tuncer *et al.* (1990); -o-: Akbari and Price (2003)

Figure 7 Drag coefficients versus angle of attack for the NACA 0012 airfoil

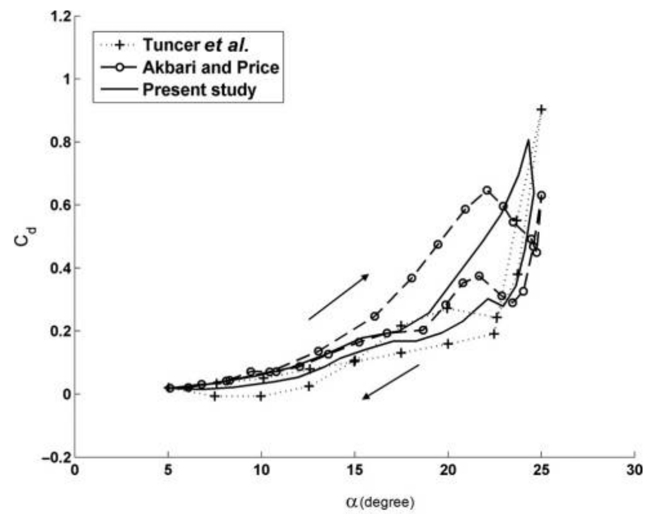

Notes: k = 0.25, Re = 10,000, α_{mean} = 5° and α_{amp} = 20°; –: present study; ..+..: Tuncer *et al.* (1990); -o-: Akbari and Price (2003)

Case 4: dynamic stall – Eppler 387

Now, the oscillations of E387 airfoil with k = 2.0, Re = 3,000, α_{mean} = 15° and α_{amp} = 30° are studied. Figure 8 shows the time elevation of the unsteady wake past the airfoil. The difference of the wake patterns between the general insight of dynamic stall behavior and E387, especially at the shedding period, is clear. The initial wake follows an unsteady process consisting of the development of the large-scale leading-edge vortex over the upper surface. Also, some small vortices can be

Figure 8 Streamline plots for the E3987 airfoil

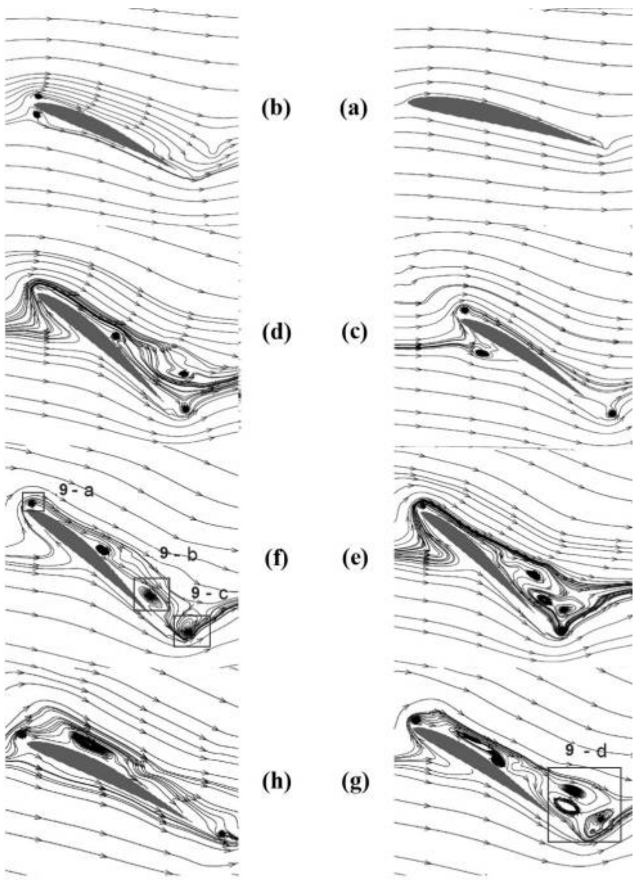

Notes: (a) $t^*=0.0$, $\alpha=15.0°$; (b) $t^*=0.1$, $\alpha=26.7°$; (c) $t^*=0.2$, $\alpha=36.5°$; (d) $t^*=0.3$, $\alpha=42.9°$; (e) $t^*=0.4$, $\alpha=45.0°$; (f) $t^*=0.5$, $\alpha=42.3°$; (g) $t^*=0.6$, $\alpha=35.3°$; (h) $t^*=0.7$, $\alpha=25.0°$; Re = 3,000; k = 2.0

observed at the down and also at the tip of the airfoil at the pitching up time. The main vortex is broken down to some smaller ones and do not leave completely the upper surface until the end of dynamic stall process. The primary and the large vortices have clockwise rotations; but the trailing edge vortices have both clockwise and counterclockwise rotations. The curl flow at the tip of the airfoil should be because of the asymmetric shape of E387 in the front area. Figure 9 shows enlarged sections of some of the main vortices in Figure 8. Figure 10 shows the non-dimensional pressure contours around the airfoil. Darker color means lower pressure. It can be seen that the high pressure area develops gradually at the pitching up time under the airfoil, but fades in the pitching down cycle.

Reduced frequency effect

In the present section, the E387 airfoil which oscillates at Re = 3,000, $\alpha_{\text{mean}} = 15°$ and $\alpha_{\text{amp}} = 30°$ is considered. Four reduced frequencies of k = 0.2, 0.5, 1.0 and 2.0 are concerned. Figures 11 and 12 show the comparisons of the drag and lift coefficients during the oscillation cycle. It is observed that the dropping of both coefficients at the maximum angle of attack

Figure 9 Enlarged sections of some main vortices patterns of the E3987 airfoil in Figure 11(f) and (g)

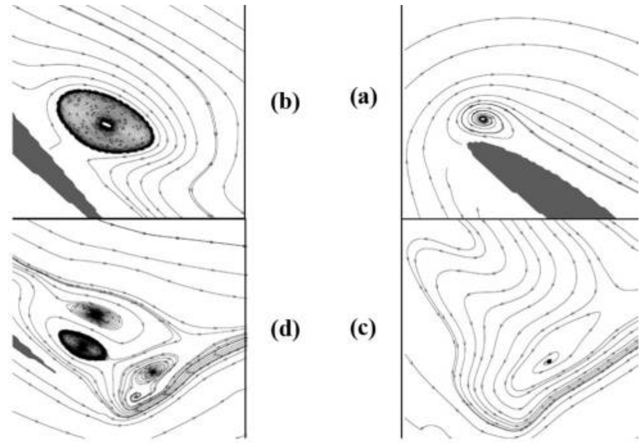

Notes: (a) Initial leading-edge vortex; (b) large-scale upper surface vortex; (c) trailing edge vortex; (d) breakdown vortices

Figure 10 Non-dimensional pressure contours for the E3987 airfoil

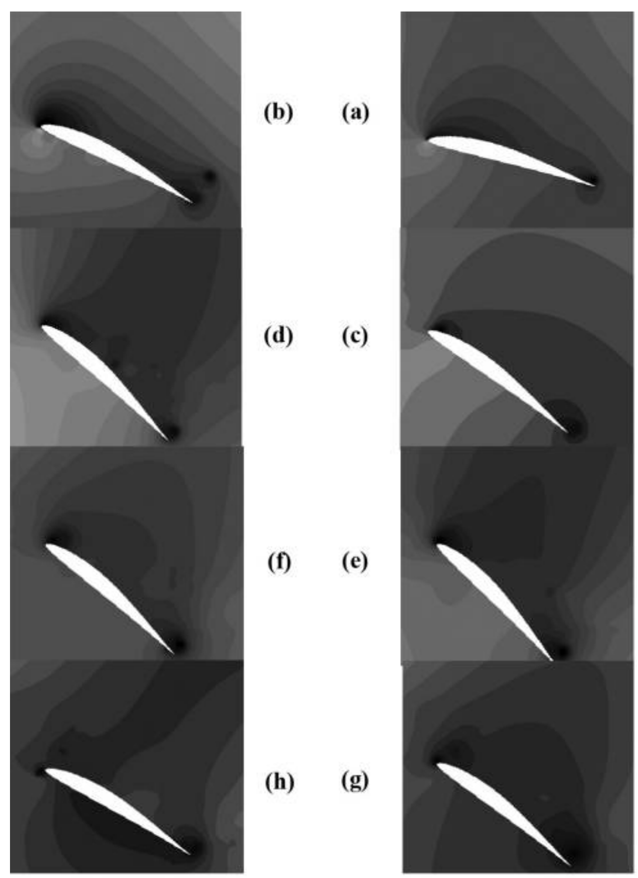

Notes: (a) $t^*=0.0$, $\alpha=15.0°$; (b) $t^*=0.1$, $\alpha=26.7°$; (c) $t^*=0.2$, $\alpha=36.5°$; (d) $t^*=0.3$, $\alpha=42.9°$; (e) $t^*=0.4$, $\alpha=45.0°$; (f) $t^*=0.5$, $\alpha=42.3°$; (g) $t^*=0.6$, $\alpha=35.3°$; (h) $t^*=0.7$, $\alpha=25.0°$; Re = 3,000; $k=2.0$

Figure 11 Drag coefficients versus angle of attacks for the E387 airfoil

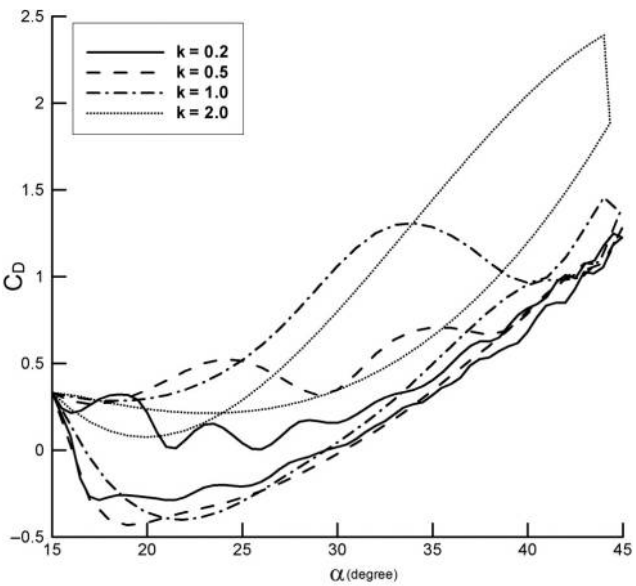

Note: Re = 3000; in different values of the reduced frequencies

Figure 12 Lift coefficients versus angle of attacks for the E387 airfoil

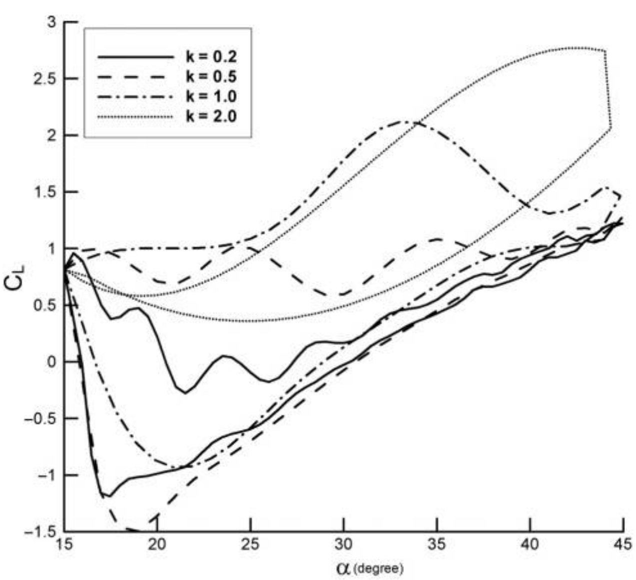

Note: Re = 3000; in different values of the reduced frequencies

significantly depend on the value of the reduced frequency. For example, in $k = 2.0$, C_D and C_L drop almost 26 and 34 per cent respectively, but in $k = 1.0$ they are almost 6 per cent. The trend is reversed at the minimum angle of attack. When the reduced frequency is less than 1.0, the rate of the changing of the coefficients are almost close; but when the reduced frequency is increased, the nonlinearity effects are dominant and the surface forces have larger values. The same results have been reported for the low-Reynolds-number airfoils (but not the E387), such as those by Ohmi *et al.* (1991) and Akbari and Price (2003). This difference also can be seen in the flow field around the airfoil. Table II shows the variation of the main wake patterns in different values of k. The details of the classified patterns are explained as follows:

- *Type A*: The leading-edge vortex after being separated from the upper surface [please see Figures 8(b) and 9(a)].
- *Type B*: The large-scale upper surface vortex detaches from the airfoil slowly of breakdown and spread over the surface [please see Figure 9(b)].
- *Type C*: The down leading-edge vortex [please see Figure 8(b)].
- *Type D*: The trailing edge vortex that can be combined with the leading-edge vortices and finally sheds downstream [please see Figures 8(c) and 9(c)].
- *Type E*: The breakdown vortices that are usually created from the large-scale vortex and generally combined with the trailing edge vortex and finally separate the airfoil [please see Figures 8(g) and 9(d)].

As it can be seen from the table, the patterns in the large values of k are more complex than the smaller ones. When the reduce frequency is less than 1.0, the main wake patterns are close to the other airfoils such as NACA 0012 case (Ohmi *et al.*, 1991), but in the shedding period, the large scale vortex does not separate the airfoil surface until the end of the cycle. Also, the leading edge and the large scale vortices are created. But at higher values, different types of vortices are created, combined and finally separated from the airfoil. In the larger ks, the vortices are clockwise and counterclockwise.

Pitch oscillation amplitude effect

Now, the effect of the pitch oscillation amplitude on the dynamic stall behavior of the E387 airfoil is studied. The case of Re = 3,000, $\alpha_{mean} = 15°$ and $k = 2.0$ is considered. α_{amp} is changed from 15° to 45°. The main wake patterns are almost same in all cases, but the periodic small vortices from the two edges are enlarged. Also, the downstream wakes are more complex and spread. An example can be seen in Figure 13 [in comparison with Figure 8(f)]. It should be noted that this change is dependent on the value of the reduced frequency (Ohmi *et al.*, 1991). The dynamic drag and lift loops also change with an increase in the amplitude. As it is expected, the maximum values of both coefficients increase with increasing of the amplitude; but the dropping values of them decrease. Also, to show that the significant coefficients drop happened after

Table II Variation of the main wake patterns in different values of the reduced frequencies

Reduced frequency	Main patterns
0.2	A → A and B → A
0.5	A and C → A → A and B → A
1.0	A and B → A and C → A and D → A and B and D → E → A and B → A
2.0	A and C → A and C and B → A and B and D → E → A and B and D → A

Notes: A: leading-edge vortex; B: large-scale vortex; C: down leading-edge vortex; D: trailing edge vortex; E: breakdown or combined vortices

Figure 13 Streamline plot for the E3987 airfoil

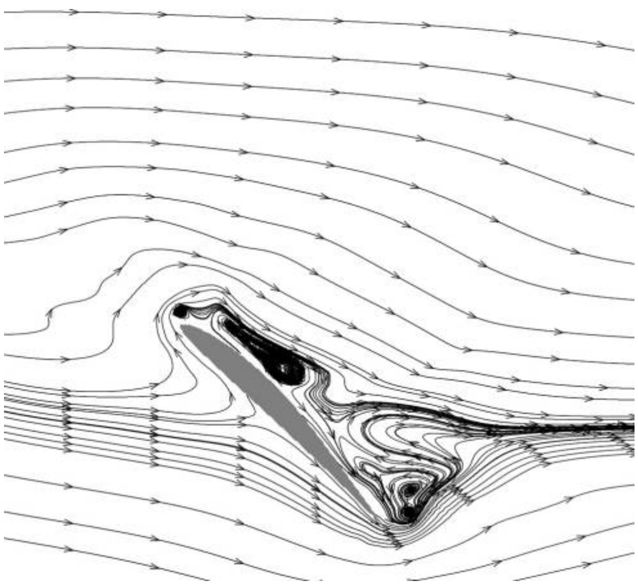

15°, another case with α_{mean} = 5°, k = 2.0 and α_{amp} = 15° is considered. In comparison with the other cases, the change in coefficients is not remarkable (Table III). In the table, the drops of C_L and C_D mean the percentage of the dropping when the pitching down cycle is started.

Reynolds number effect

In the last section, the effect of the Reynolds number on the dynamic stall behavior of the E387 airfoil is studied. In all cases, α_{mean} = 15°; α_{amp} = 30° and k = 2.0. Three Reynolds numbers in the laminar fluid flow regime are selected: 1,500, 3,000 and 10,000. In general, the effect of the Reynolds number is small compared to other parameters. The basic wake patterns are almost the same. Some local fluctuations are observed at Re = 10,000, but they fade very fast. It should be noted that the present model is valid for low Reynolds numbers, and the absence of the turbulent model should be the main reason of the distortions. Also, the coefficients loops are almost similar, and no significant differences are seen (Figure 14).

Conclusions

A validated modified DFIB method has been used for simulating dynamic stall behavior of the Eppler 387 airfoil in the low Reynolds number regime. The ray-casting method has been established to define the airfoil geometry. Grid convergence test was carried out for the static airfoil, and the results demonstrate that the model provides reasonably accurate predictions of the lift and drag coefficients for most of the selected cases. Next, a dynamic stall case of the NACA 0012 has been considered. The good similarities were seen in the force loops. Next, The E387 dynamic stall behavior was studied. The wake patterns were discussed in detail. Finally, three main parameters in this phenomenon reduced frequency; pitch oscillation amplitude and the Reynolds number were considered. The results showed that the reduced frequency has the major effect on the flow field and the force coefficients of the airfoil. Results are in good agreements with the former studies. However, it was observed that the wake patterns at the shedding period and the main force coefficients are different. Eventually, it can be concluded that the combination of the DFIB method and the ray-casting algorithm offers considerable promise as a numerical technique for simulating flow interaction with a complex solid geometry.

Table III Drag and lift coefficients characteristics in different value of the pitch oscillation amplitude

α_{amp}	Maximum C_D	Drop C_D (%)	Maximum C_L	Drop C_L (%)
15	0.95	75	1.60	75
30	2.40	26	2.80	34
45	4.60	25	3.30	40
15 (α_{mean} = 5°)	0.63	5	1.32	8

Figure 14 Lift coefficients versus angle of attacks for the E387 airfoil at different values of the Reynolds numbers

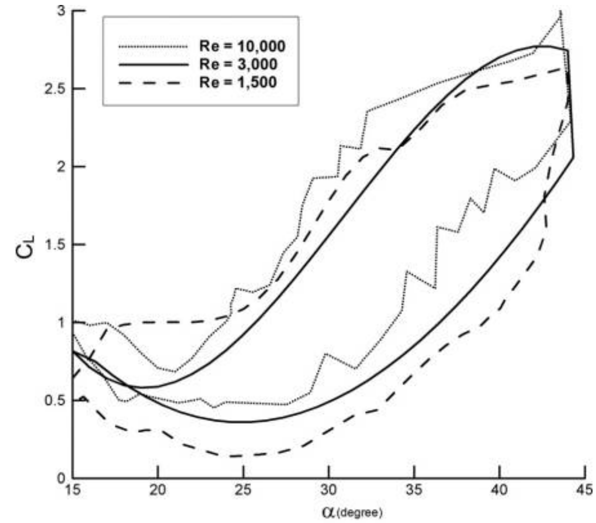

Note: k = 2.0

References

Akbari, M.H. and Price, S.J. (2003), "Simulation of dynamic stall for a NACA 0012 airfoil using a vortex method", *Journal of Fluids and Structures*, Vol. 17 No. 6, pp. 855-874.

Delouei, A.A., Nazari, M., Kayhani, M.H., Kang, S.K. and Succi, S. (2016), "Non-newtonian particulate flow simulation: a direct-forcing immersed boundary–lattice Boltzmann approach", *Physica A: Statistical Mechanics and its Applications*, Vol. 447, pp. 1-20.

Belliard, M., Chandesris, M., Dumas, J., Gorsse, Y., Jamet, D., Josserand, C. and Mathieu, B. (2016), "An analysis and an affordable regularization technique for the spurious force oscillations in the context of direct-forcing immersed boundary methods", *Computers & Mathematics with applications*, Vol. 71 No. 5, pp. 1089-1113.

Chern, M.J., Kuan, Y.H., Nugroho, G., Lu, G.T. and Horng, T.L. (2014), "Direct-forcing immersed boundary modeling of vortex-induced vibration of a circular cylinder", *Journal of Winds Engineering and Industry Aerodynamics*, Vol. 134, pp. 109-121.

Chern, M.J., Zulhidayat Noor, D., Liaoand, C.B. and Horng, T.L. (2015), "Direct-forcing immersed boundary method for mixed heat transfer", *Communications in Computational Physics*, Vol. 18 No. 4, pp. 1072-1094.

Eshghinejadfard, A., Abdelsamie, A., Janiga, G. and Thévenin, D. (2016), "Direct-forcing immersed boundary lattice boltzmann simulation of particle/fluid interactions for spherical and non-spherical particles", *Particuology*, Vol. 25, pp. 93-103.

Gardner, A.D., Wolf, C.C. and Raffel, M. (2016), "A new method of dynamic and static stall detection using infrared thermography", *Experiments in Fluids*, Vol. 57 No. 9, p. 149.

Ko, S. and McCroskey, W. (1997), "Computations of unsteady separating flows over an oscillating airfoil", *AIAA J*, Vol. 35 No. 7, pp. 1235-1238.

Lee, T. and Gerontakos, P. (2004), "Investigation of flow over an oscillating airfoil", *Journal of Fluid Mechanics*, Vol. 512, pp. 313-341.

Leonard, B.P. (1979), "A stable and accurate convective modelling procedure based on quadratic upstream interpolation", *Computational Methods in Applied Mechanics Engineering*, Vol. 19 No. 1, pp. 59-98.

McCroskey, W. (1981), "The phenomenon of dynamic stall", Technical report, NASA TM-81264.

McCroskey, W. (1982), "Unsteady airfoils", *Annual Review of Fluid Mechanics*, Vol. 14 No. 1, pp. 285-311.

McGhee, R.J., Walker, B.S. and Millard, B.F. (1988), "Experimental results for the Eppler 387 airfoil at low Reynolds numbers in the Langley Low-Turbulence pressure tunnel", NASA technical memorandum 4062.

Mohan, A.T., Gaitonde, D.V. and Visbal, M.R. (2016), "Model reduction and analysis of deep dynamic stall on a plunging airfoil", *Computers & Fluids*, Vol. 129, pp. 1-19.

Mohd-Yusof, J. (1996), "Interaction of massive particles with turbulence", PhD. Dissertation, Dept. of Mechanical and Aerospace Engineering, Cornell University, USA.

Noor, D.Z., Chern, M.J. and Horng, T.L. (2009), "An immersed boundary method to solve fluid-solid interaction problems", *Computational Mechanics*, Vol. 44 No. 4, pp. 447-453.

Ohmi, K., Coutanceau, M., Phuoc Loc, T. and Dulieu, A. (1991), "Further experiments on vortex formation around an oscillating and translating airfoil at large incidences", *Journal of Fluid Mechanics*, Vol. 225 No. 1, pp. 607-630.

Peskin, C.S. (1972), "Flow patterns around heart valve: a numerical method", *Journal of Computational Physics*, Vol. 10 No. 2, pp. 252-271.

Shahin, M., Hall, J., Mohseni, K. and Hillewaert, K. (2008), "Direct numerical simulation of separated low-Reynolds number flows around an Eppler 387 airfoil", *46th AIAA Aerospace Science Meeting*, *American Institute for Aeronautics and Astronautics (AIAA)*, *Nevada*.

Sutherland, I., Sproull, R.F. and Schumacker, R.A. (1974), "A characterization of ten hidden-surface algorithms", *ACM Computing Surveys*, Vol. 6 No. 1.

Tuncer, I.H., Wu, J.C. and Wang, C.M. (1990), "Theoretical and numerical studies of oscillating airfoils", *AIAA J*, Vol. 28 No. 9, pp. 1615-1624.

Wang, S., Ma, L., Ingham, D., Pourkashanian, M. and Tao, Z. (2010), "Numerical investigations on dynamic stall of low Reynolds number flow around oscillating airfoils", *Computer and Fluids*, Vol. 39 No. 9, pp. 1529-1541.

Further reading

Xfoil subsonic airfoil development system, web.mit.edu/drela/Public/web/xfoil

Corresponding author

Nima Vaziri can be contacted at: nima_vaziri@kiau.ac.ir